GIA NEWS FROM RESEARCH

This report provides a status update for an ongoing research project at GIA. Comments on the direction of this and other projects are warmly welcomed, as are offers of collaboration. Contact information can be found in the "About the Authors" section on page 18.

Sapphires from Anakie, Australia:

A closer look at blue, yellow, green and bicolor sapphires

Sudarat Saeseaw, Wim Vertriest, and Aaron Palke

This variety of sapphire colors is typical for the Anakie gemfields in Eastern Australia. Courtesy of Fura Gems.

Australian Sapphires

INTRODUCTION

Australia has a long and rich sapphire mining history, yet the blue gems from Down Under have rarely been fully appreciated. While they were most desired in the early 1900s, their position has faded to the background. That doesn't mean that mining stopped; both large and small operations kept operating in the last decades.

Recent efforts have cast a new light on the variety of sapphires in Australia, which includes classic blues and yellow, green, and bicolor stones. This suite of colors is also referred to as BGY sapphires, which are classically related to alkali-basalt eruptions.

In this study, we take a deeper look at the colors of these sapphires and what caused them, as well as the inclusion scenes observed in these gems.

HISTORY AND GEOLOGY

The story of Australian sapphires starts with a few flecks of gold found in a stream in New South Wales in 1851. This chance discovery of gold set off a number of rushes in Australia, with prospectors scattering across the great Australian outback seeking their fortunes in unexplored mineral deposits. In the same year, gold prospectors reported sapphires found during gold mining along the Cudgegong and Macquarie Rivers in New South Wales. The famous Inverell sapphire deposit was also found by gold seekers in 1854. These early gem finds did not prove enough of a distraction for the early gold miners, with the first commercial production of Australian sapphires still two decades off. In 1875, Archibald John Richardson, a surveyor for the railroad, sent off some red zircons for testing, which he had found while working on Retreat Creek near the town of Anakie in Queensland. He may have thought these stones were rubies, but he evidently missed the sapphires he produced alongside the zircons. Once the sapphires were identified, Mr. Richardson and partners formed a company to mine these gems, with the first commercial production in 1891 (Dunstan, 1902).

The first few decades up to the end of the First World War were very lucrative. The rich Anakie gem fields were exceptionally productive, and the blue sapphires produced found an easy market among German gem dealers who cut the stones and sold them to the Russian Imperial Court, where the deep and darker tone of these Australian sapphires was in favor. The end of Imperial Russia in 1917 and the First World War that tore through Europe caused demand for Australian sapphires to collapse, and production at Anakie virtually ground to a halt (Coldham, 1985).

Resurgent demand from the burgeoning gem industry in Thailand in the early 1960s brought sapphire mining back to Anakie (Coldham, 1985). Initially, Australia was a dominant force in the sapphire mining industry, but rising production in East Africa and Asia reduced the global importance of the deposits in New South Wales and Queensland. Nevertheless, several small-scale operations have persisted as well as a few larger mechanized operations (figures 1-4) that provided Australian sapphires to the domestic and Asian market. The most recent development in this area is the renewed interest in large-scale mining and the promotion of Australian sapphires with the arrival of Fura Gems, who now hold a combined 20.23 km^2 mining licenses in the rich deposits between the towns of Rubyvale and Sapphire. With a focus on securing a responsible and traceable route from the mine to the market, the entry of Fura Gems to the Anakie deposits has the potential to bring Australian sapphires back into the spotlight.

Figure 1. Small-scale operations still rely heavily on mechanization with digging and washing equipment that is more advanced than what is seen in similar-sized operations on other continents. Photo by V. Pardieu/GIA.

Figure 2. At large-scale operations, heavy equipment is used to expose the sapphire-bearing layers. Australia's strict mining practices require topsoil to be preserved, so this is dug out before the actual gem-rich layers are touched. Photo by V. Pardieu/GIA.

Figure 3. While the systems used in large-scale operations are similar to those run by a single person, the size sets them apart. Large washing plants can handle several metric tons of ore per hour and often run around the clock. This equipment requires a lot of water, so it is common to find manmade settling ponds nearby. Photo by V. Pardieu/GIA.

Geology

Most commercial production of Australian sapphires has come from the Anakie deposit in Queensland and the Inverell (New England) deposit in New South Wales. However, sapphires (and very rarely rubies) have been found in multiple locales all along the eastern seaboard of Australia, from Tasmania in the south to Lava Plains in northern Queensland (Sutherland and Webb, 2007). These deposits are all closely associated with voluminous eruptions of alkali basalts that erupted relatively recently in geological time in the Cenozoic Era. In fact, the youngest of these deposits at Lava Plains is related to basalts that are only 20,000 to 3 million years old, whereas basalts in the Anakie deposit date to 15–81 million years ago (Sutherland et al., 2015). While many mysteries remain about the ultimate origin of these sapphires, a few things are well understood. The sapphires are apparently xenocrysts in the basalts, meaning that they did not crystallize out of the basalts. The basalts acted simply as the transport mechanism from some unknown depths of the earth. The sapphires themselves possibly formed near the crust/mantle boundary through the intrusion of alkali-rich magmas such as syenites. This is reflected in the common presence of feldspar crystals and other inclusions suggesting a magmatic origin.

This type of deposit is found in numerous localities throughout the world and probably accounts for the highest volume of sapphires globally. Some of the most productive basalt-related sapphire deposits are found in Australia, Nigeria, Thailand, and China.

Figure 4. Heavy equipment is used to extract the weathered basalt layers. Over time, they have turned into reddish sands and clays, which can be easily dug out with an excavator without the use of explosives. In some cases, river systems have washed away the sands and only left behind the heavy minerals, including sapphires. Photo by V. Pardieu/GIA.

MATERIALS AND METHODS

Ninety samples from FURA's mining license in the Anakie gemfields were randomly selected for this study. Color ranged from blue to dark blue, yellowish green, yellow, and greenish yellow to brownish yellow, as shown in Figure 5.

Five samples were fabricated with windows perpendicular to the c-axis for spectroscopy to obtain ordinary or o-ray spectra. Standard gemological instruments were used to measure refractive index, birefringence, specific gravity, and visible absorption spectra. A long-wave (365 nm) and short-wave (254 nm) ultraviolet lamp was used for fluorescence observations. Microscopic observations were captured at different magnifications with a Nikon SMZ 18 system and a Nikon SMZ 1500 system using darkfield, brightfield, diffused, and oblique illumination, together with a fiber-optic light source when necessary.

Figure 5. Some of the studied samples from Australia. Colors ranged from blue to dark blue, yellowish-green, yellow, and greenish yellow to brownish yellow. Photo by Lhapsin Nillapat.

Ultraviolet/visible/near-infrared (UV-Vis-NIR) spectra were collected with a Hitachi U-2910 spectrophotometer with a polarizer accessory. A wavelength resolution of 1.5 nm was used. Fourier-transform infrared (FTIR) spectroscopy was performed using a Thermo Nicolet 6700 FTIR spectrometer equipped with an XT-KBr beam splitter and a mercury-cadmium-telluride (MCT) detector operating with a 4× beam condenser accessory. To identify mineral inclusions, Raman spectra were obtained using a Renishaw inVia Raman microscope fitted with a 514 nm argon-ion laser.

Laser ablation–inductively coupled plasma–mass spectrometry (LA-ICP-MS) analyses were conducted on a Thermo Scientific iCap-Q ICP-MS with plasma RF power of 1400 W coupled with a New Wave Research UP-213 laser ablation unit with a frequency-quintupled Nd:YAG laser (213 nm wavelength with 4 ns pulse width). Laser conditions consisted of a 55 µm diameter spot size, a fluence of 10±1 J/cm^2, and a 15 Hz repetition rate using internally developed corundum standards (Stone-Sundberg et al., 2018).

GEMOLOGICAL PROPERTIES

Sapphires from Australia had colors ranging from blue, green, yellow, brown, or parti-colored with mixtures of blue and yellow. The blue sapphires have hues ranging from green-blue to blue with medium-dark to very-dark tones and a wide range of saturations (slightly grayish/brownish to vivid). Green sapphires have mostly yellowish green hues with medium to medium-dark tones and strong saturation. Finally, the hues of yellow sapphires are generally very slightly greenish yellow with medium to dark tone and strong to vivid saturation. Typical refractive index was between 1.762 and 1.773 with a birefringence of 0.008–0.009, consistent with gem corundum. All samples were inert under both long- and short-wave UV radiation.

Inclusions/Microscopic Observations

The internal world of Australian sapphires is very diverse and astonishing when observed through a microscope. The scenes are dominated by a variety of growth textures as well as crystalline inclusions. Especially common are angular or hexagonal growth features composed of minute particles and/or fine-grained clouds (figures 6–9). Crosshatch or flake-like inclusions and stringers are sometimes observed (figures 10–13) but tend to be rarer.

When you look closer at the particles, they too exhibit different features. Some are long intersecting rutile needles with a typical straight and slender appearance, while others are reflective ilmenite needles and platelets that tend to be a bit more irregular and stubbier (figures 14 and 15).

Negative crystals associated with iridescent fluid inclusions can often show a spectacular display of interference colors when they are correctly illuminated (figure 16). This illumination environment can also reveal tiny crystals with equatorial thin films, sometimes referred to as “fried egg” inclusions (figure 17). These inclusions are commonly found in gem corundum from a basalt-related deposit.

In a few sapphires, lamellar twinning planes can be seen, often associated with tubules and fingerprints (figures 18 and 19). Also noticed are opaque black inclusions, sometimes occurring as single crystals, other times as trails of crystals (figures 20 and 21). Different shapes of feldspar (figure 22) and sapphire inclusions (figure 23) are the other solid crystal inclusion observed.

Brownish yellow or greenish yellow sapphires have some different inclusions different from those found in blue Australian sapphires. They typically showed reflective ilmenite needles or brown particles, compared to the long slender rutile needles seen in the blue sapphires (figures 24 and 25). Also seen are stringers of satellite-like inclusions (figure 26) and lamellar twinning associated with tubules (figure 27).

Most of the inclusions seen in Australian sapphires are extremely similar to those observed in sapphires from other basalt-related deposits (Palke et al., 2019). Geographic origin determination for Australian sapphires often relies heavily on trace element chemistry measurements (see below), but this analysis brings its own challenges.

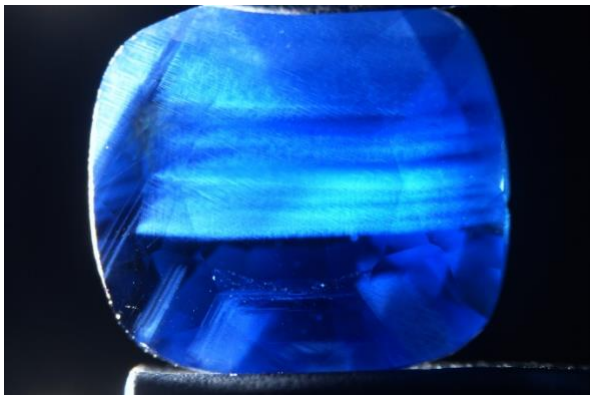

Figure 6. Angular bands of flaky inclusions are commonly seen. Photomicrograph by Charuwan Khowpong; field of view 9.6 mm.

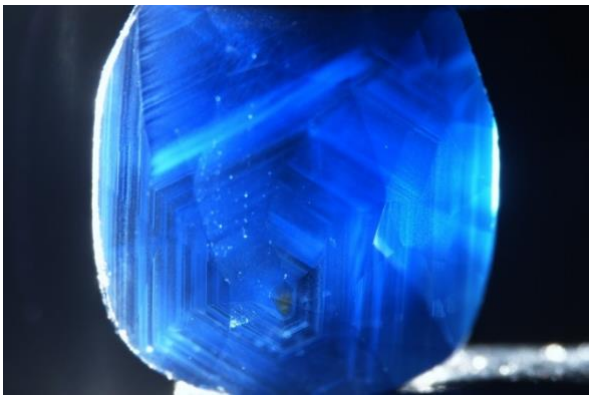

Figure 7. In some cases, a perfect hexagonal growth pattern can be seen. Photomicrograph by Charuwan Khowpong; field of view 7.2 mm.

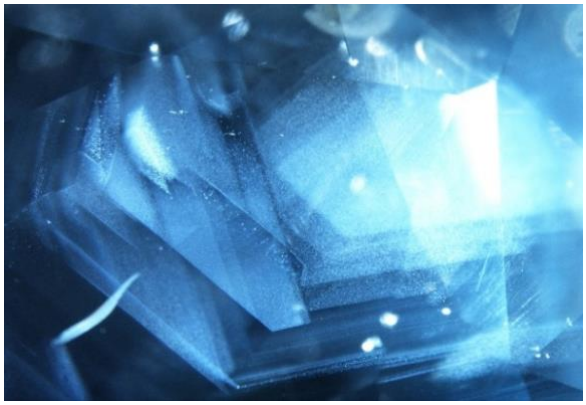

Figure 8. A close-up of some particle clouds reveals the hexagonal pattern with straight edges and 120° angles. Photomicrograph by Ungkhana Atikarnsakul; field of view 4 mm.

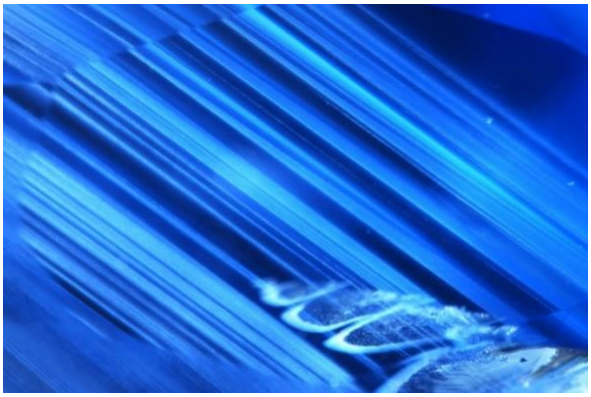

Figure 9. Milky bands alternate with fine particle zones. In the bottom right, a trail of healed fractures around tiny crystals can be seen. Photomicrograph by Charuwan Khowpong; field of view 2.85 mm.

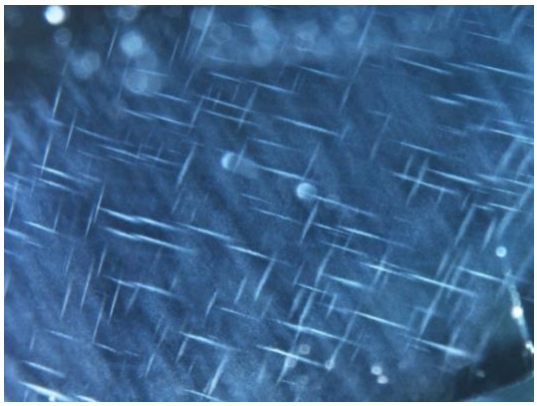

Figure 10. Crosshatch inclusions form patterned clouds that can take on various dimensions in the sapphires. Photomicrograph by Ungkhana Atikarnsakul; field of view 2 mm.

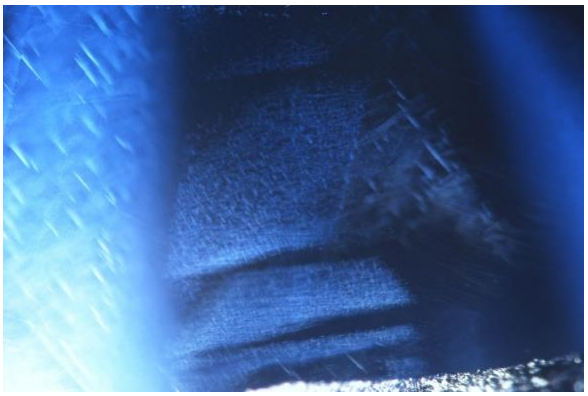

Figure 11. In this image, large and small crosshatch inclusions appear next to each other, highlighting their variable size. Photomicrograph by Charuwan Khowpong; field of view 2.85 mm.

Figure 12. Flake inclusions in milky bands. Photomicrograph by Charuwan Khowpong; field of view 2.4 mm.

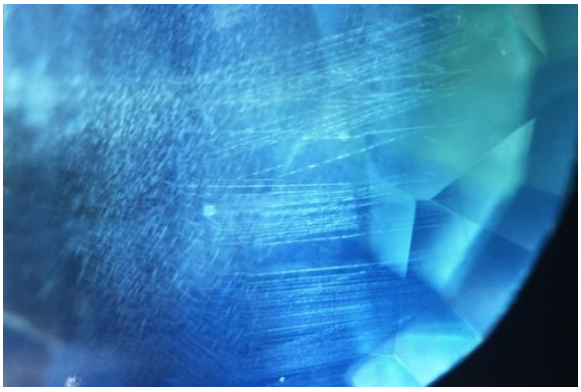

Figure 13. Fine crosshatch pattern associated with stringers. Photomicrograph by Charuwan Khowpong; field of view 3.65 mm.

Figure 14. Rutile particles occur in various sizes and densities throughout this sapphire. Photomicrograph by Ungkhana Atikarnsakul; field of view 8.2 mm.

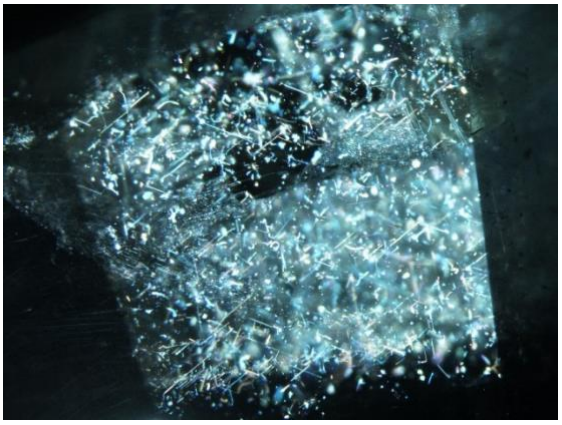

Figure 15. Irregularly shaped reflective platelets of ilmenite. Photomicrograph by Ungkhana Atikarnsakul; field of view 2 mm.

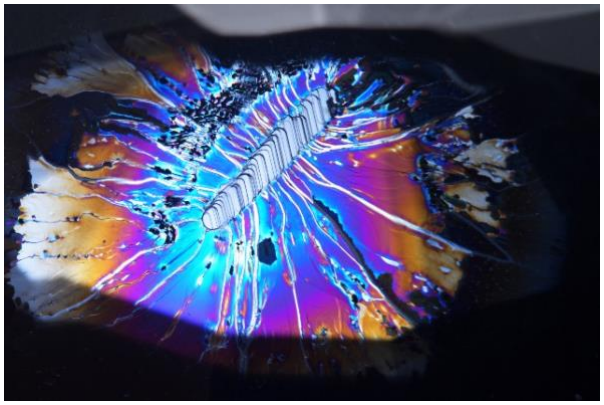

Figure 16. When correctly illuminated, these fractures can show iridescent colors. Photomicrograph by Charuwan Khowpong; field of view 2 mm.

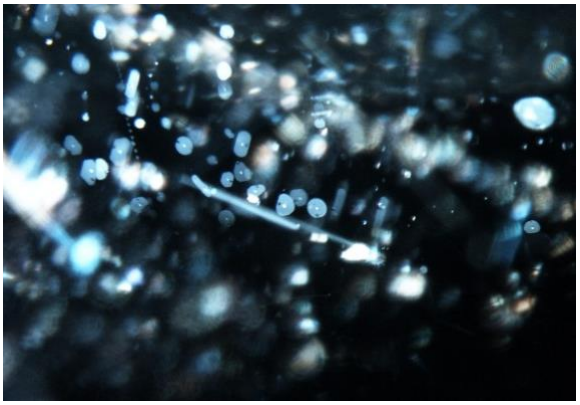

Figure 17. Tiny crystals with equatorial thin films are sometimes referred to as “fried-egg” inclusions. Photomicrograph by Ungkhana Atikarnsakul; field of view 3.1 mm.

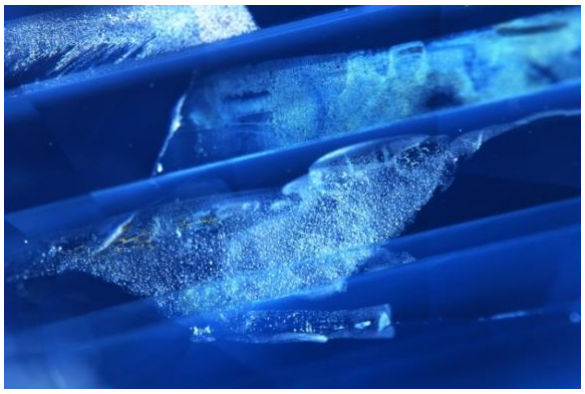

Figure 18. Several sapphires showed obvious twinning planes. In this case, they are associated with naturally healed fractures. Photomicrograph by Charuwan Khowpong; field of view 3.65 mm.

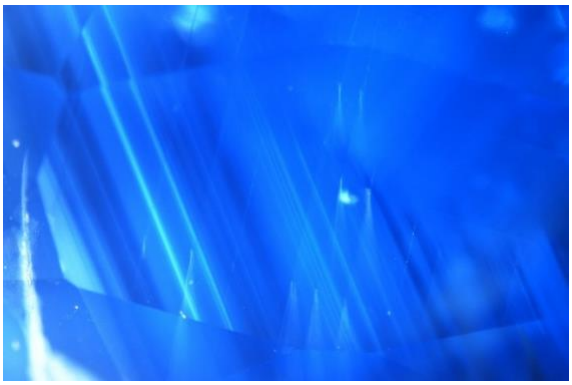

Figure 19. Some of the lamellar twinning is associated with tubules. Photomicrograph by Charuwan Khowpong; field of view 3.65 mm.

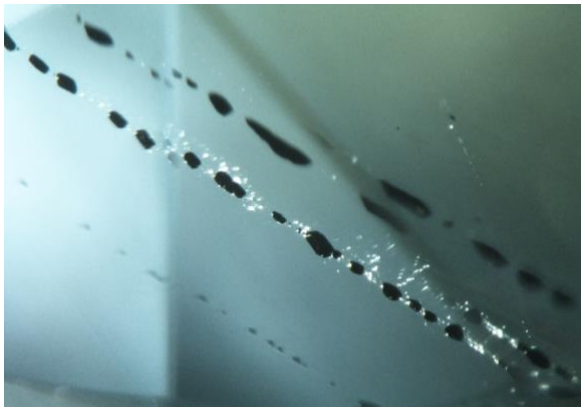

Figure 20. Strings of opaque black crystals can be seen in some of the sapphires. In this case, they were identified as chromite. Photomicrograph by Charuwan Khowpong; field of view 1.3 mm.

Figure 21. An unidentified opaque black crystal with a fracture. Photomicrograph by Ungkhana Atikarnsakul; field of view 1.5 mm.

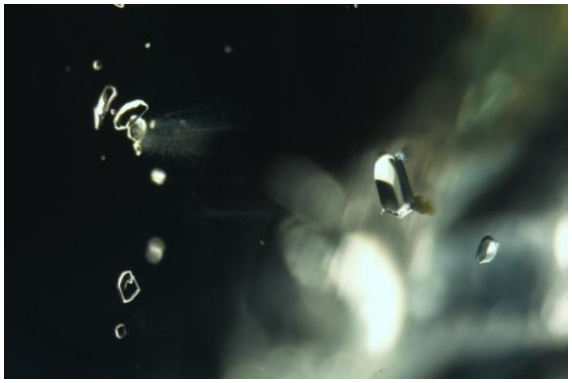

Figure 22. Feldspar crystals are common in all sapphires but can appear in various shapes, as seen in this sample. Photomicrograph by Charuwan Khowpong; field of view 4.8 mm.

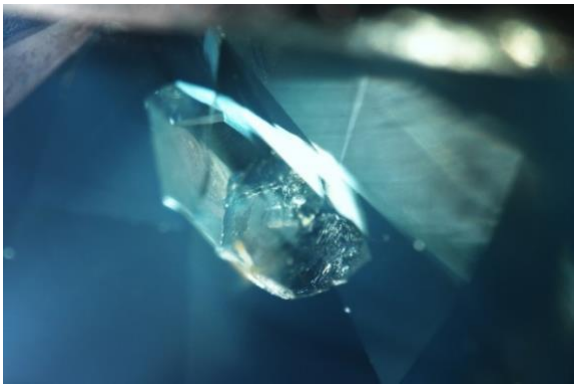

Figure 23. In some rare cases, colorless sapphire can be seen as an inclusion in sapphire. Photomicrograph by Charuwan Khowpong; field of view 3.1 mm.

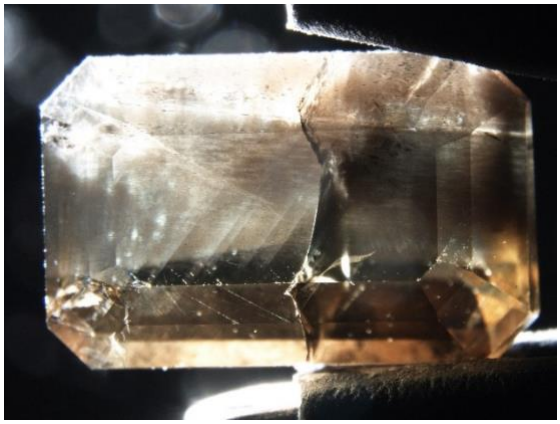

Figure 24. Green sapphires often show brown platelets of ilmenite, while blue sapphires often have more silver-colored rutile needles. Photomicrograph by Ungkhana Atikarnsakul; field of view 11 mm.

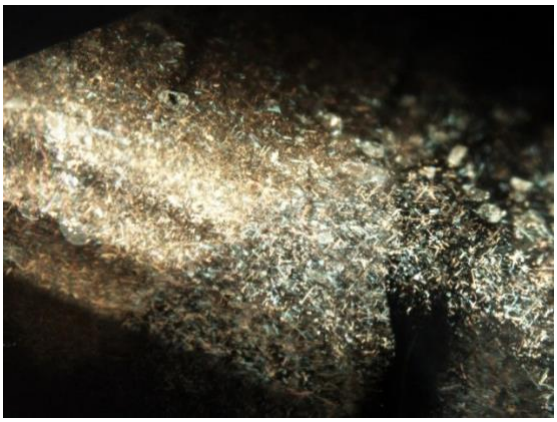

Figure 25. A further close-up on these ilmenite particles shows their irregular nature. Photomicrograph by Ungkhana Atikarnsakul; field of view 2.7 mm.

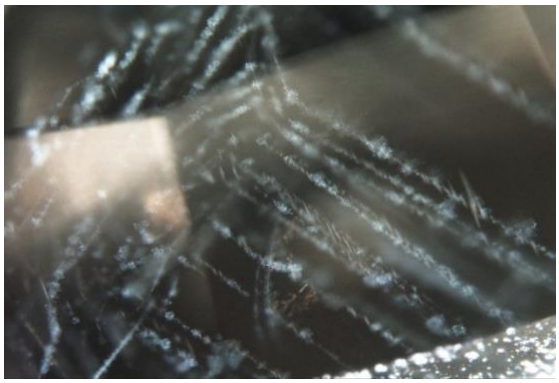

Figure 26. Strings of particles with short needles. Photomicrograph by Ungkhana Atikarnsakul; field of view 2 mm.

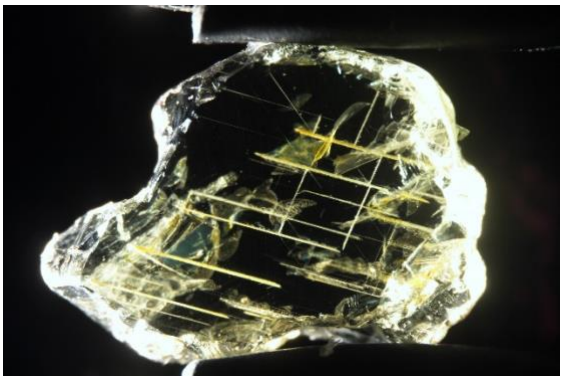

Figure 27. Lamellar twinning associated with tubules. Photomicrograph by Charuwan Khowpong; field of view 9.6 mm.

UV-Vis-NIR Spectroscopy

Gemological laboratories primarily use UV-Vis-NIR absorption spectroscopy to identify the cause of color in gemstones, but in the case of sapphire, it can also provide some clues to their geological origin.

UV-Vis-NIR spectra of blue/green/yellow Australian sapphires are shown in figure 28. Blue sapphire showed a strong absorption band of Fe^{2+}-Ti^{4+} at 580 nm, which is the cause of their blue color (Dubinsky et al., 2021). A broad band at about 880 nm is also seen, which is probably a relationship between Fe^{2+} and Ti^{4+}, Si^{4+}, or both (as described in Hughes et al., 2017, chapter 4), and is commonly seen in blue sapphires having a basaltic origin. The observation of this absorption band can help separate basalt-related sapphires from the geologically distinct metamorphic sapphires (Palke et al., 2019). Finally, absorption features related to Fe^{3+} are seen at 377, 388, and 450 nm. The Fe^{3+} absorption bands are the cause of yellow coloration in sapphires. In yellow sapphires, the Fe^{3+} peak at 450 nm is stronger than the Fe^{2+}-Ti^{4+} absorption band at 580 nm. In the case of these blue sapphires, the features that cause the

yellow color are overpowered by the Fe-Ti intervalence charge transfer (IVCT), so the overall color is blue.

In yellow sapphires, the absorption bands at 580 and 880 nm are absent. This leaves only the Fe^{3+}-related features, which cause the yellow color.

The cause of color in green sapphires is a mixture of the blue and yellow chromophores described above.

Table 1 shows the chemistry of a blue sapphire with 22 ppma Ti available to pair with Fe, producing a strong blue color. On the other hand, the yellow sapphire described in table 1 has no excess of Ti. Ti prefers to bind with Mg before making the bond with Fe. This leaves 2 ppma Mg that may be available to create a trapped hole, which could also create color. However, no significant trapped hole absorption feature was seen in the absorption spectrum of the yellow sapphire (Dubinsky et al., 2021). The yellow color seems to be solely from Fe^{3+}, without a contribution from Mg-related trapped holes. Potentially the Mg could be charge-balanced by the presence of Si, which cannot be measured by LA-ICP-MS (Emmett et al., 2017). SIMS analysis is required to answer this mystery.

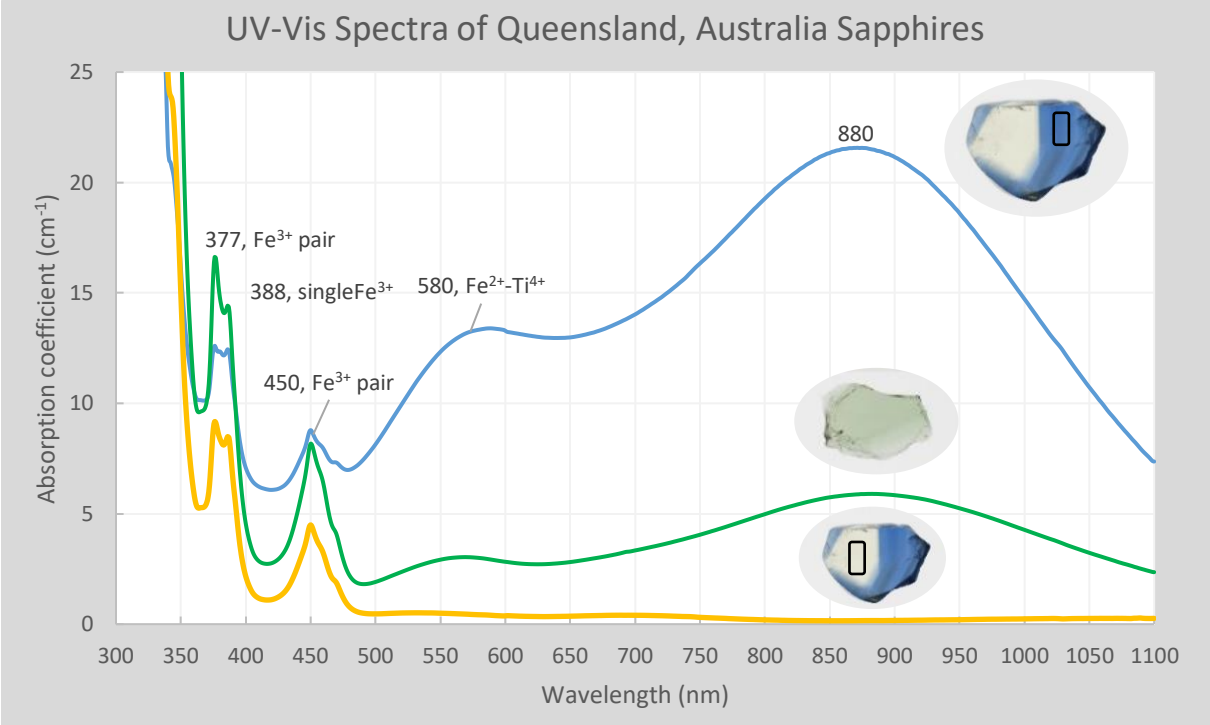

Figure 28. Comparison o-ray spectra of blue, green, and yellow Australian sapphires with inset color-calibrated polarized photos of the beam path area for each sample. Optical path lengths are 1.539 mm for blue and yellow and 2.05 mm for greenish blue sapphires.

Table 1. LA-ICP-MS results in parts per million atomic (ppma) units for samples in figure 28.

Color	^{24}Mg	^{47}Ti	[^{47}Ti] - [^{24}Mg] Or Ti available	^{51}V	^{53}Cr	^{57}Fe	^{69}Ga
Blue	4±1.1	17±3.1	13	3±0.3	BDL	1401±106	27±2
Green	6±0.5	7±1	1	5±0.6	11±1.3	2479±313	51±8
Yellow	7±0.4	5±0.5	n/a	4±0.3	BDL	1632±130	30±3

FTIR Spectroscopy

FTIR spectroscopy can be very useful in providing clues for identifying heat-treated sapphires or for understanding trace element chemistry or defects in sapphires. We categorized FTIR spectra based on color, including blue, green, greenish yellow, and bi-color blue and yellow (figure 29). All blue sapphires and the blue zones in bi-color sapphires showed a strong 3309 series, which represents hydrogen associated with titanium (Moon and Phillips, 1991). Six green sapphires showed a 3309 series, whereas four samples showed a single 3309 and one green sapphire showed no IR features. Greenish yellow sapphire showed a single 3309 cm^{-1} or no IR features. Only four bi-color samples showed a broad band in the yellow zone at 2000–3300 cm^{-1}, known as "Punsiri"-like feature (figure 30). The so-called Punsiri bands are related to hydrogen associated with excess magnesium in sapphire (Fukatsu et al., 2003). This feature was observed in heated blue sapphire but can be found in unheated yellow basalt sapphire as reported in Sangsawong et al. (2016).

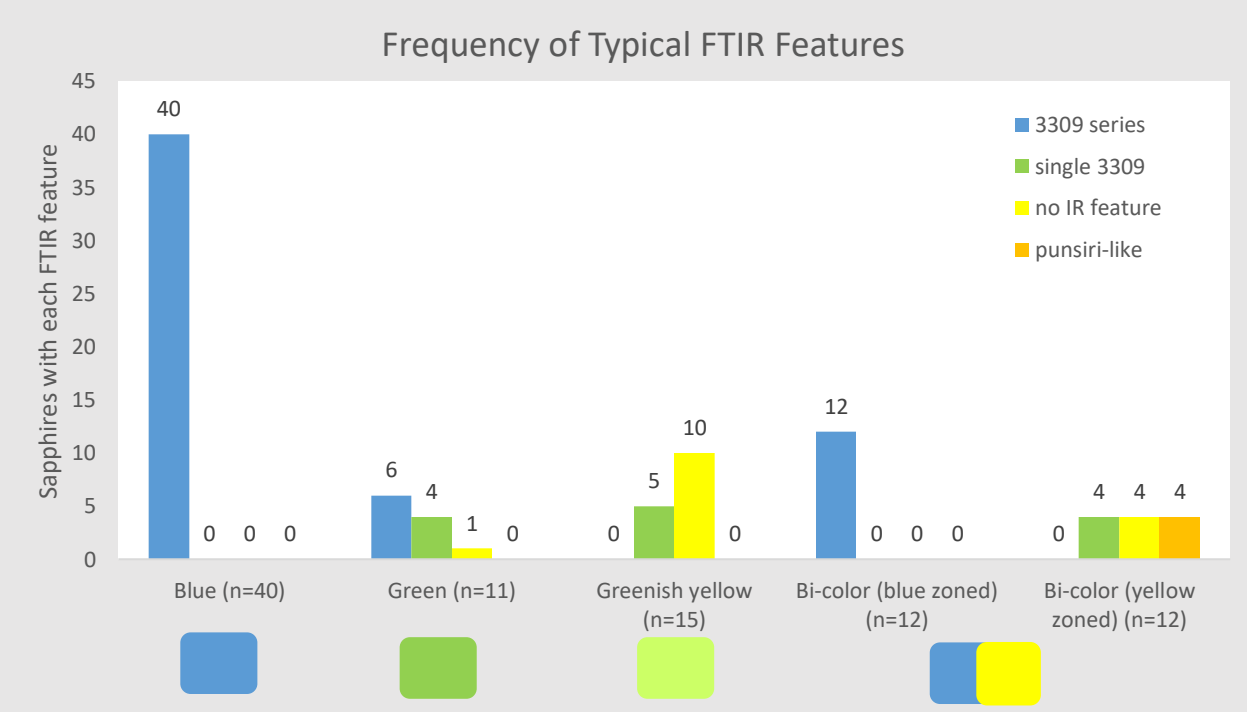

Figure 29. The distribution of FTIR spectra found in Australian sapphire of different colors.

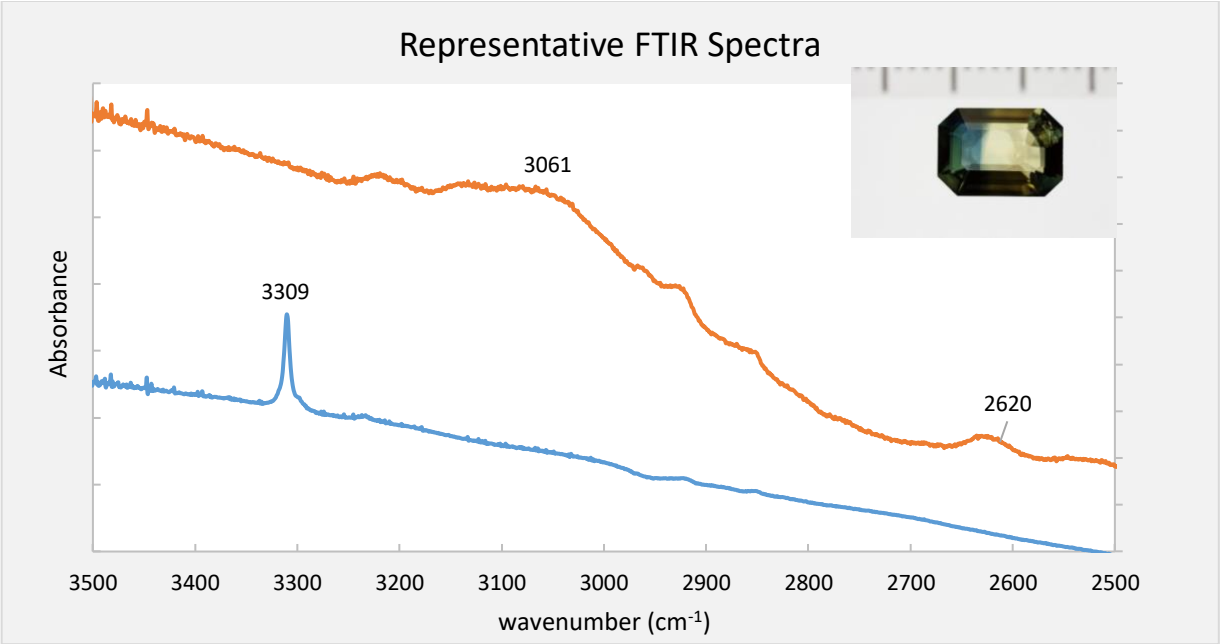

Figure 30. FTIR spectra of bi-color sapphire presenting a 3309 series in the blue zone and a broad band at 2000–3300 cm^{-1} or Punsiri-like feature in the yellow zone. [Ti]-[Mg] = 9 ppma in the blue zone and the [Mg]-[Ti] = 3 ppma in the yellow zone.

Chemistry

Australian blue sapphires have trace elements similar to those of other basalt sapphires. In this study, Mg in blue sapphires is found in a range of 2–16 ppma, Ti from 10–90 ppma, V from 2–7 ppma, Fe from 2118–3556 ppma, and Ga from 44–71 ppma. Cr was below the detection limit or lower than 1 ppma. Chemistry in greenish yellow, green, and yellow brown sapphires usually showed higher concentrations of iron (see Table 2). Compared to other important deposits of basalt-related sapphires, those from Queensland, Australia, tend to be enriched in Fe content. They are further separated from most Thai sapphires (which are also high in Fe) by the generally higher vanadium contents in Australian sapphires (figure 31). However, there is still significant overlap when considering the data on standard two-dimensional plots. In many cases, the use of advanced statistical techniques that consider trace element chemistry in multi-dimensional space, such as the so-called selective plotting method described by Palke et al. (2019), can often help separate Australian sapphires from other deposits.

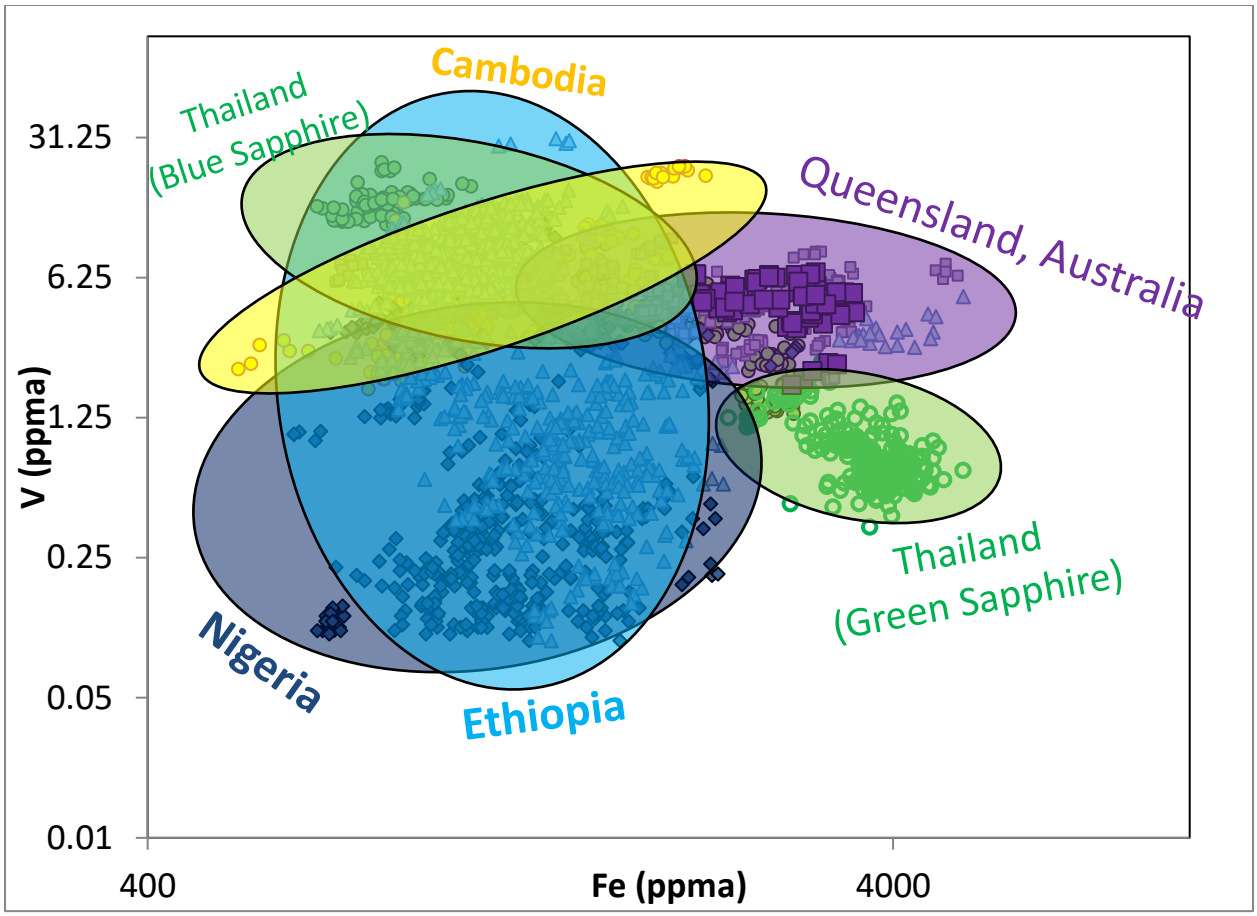

Figure 31. Plot of Fe vs. V (in ppma) showing the general range of chemistry for basalt-related sapphires from important global deposits. While there is overlap in two-dimensional plots like this, advanced statistical techniques such as the selective plotting method described by Palke et al. (2019) can often help separate Australian sapphires from other world deposits.

Table 2. LA-ICP-MS results in blue, greenish yellow, green, and yellowish brown Australia sapphires. Min ± max (average) and reported in ppma or parts per million atomic.

Color	^{24}Mg	^{47}Ti	^{51}V	^{53}Cr	^{57}Fe	^{69}Ga
Blue	2 ± 16 (5)	10 ± 91 (38)	2±6 (5)	BDL	2118 ± 3556 (2827)	44 ± 72 (52)
Greenish yellow and green	1 ± 53 (8)	2 ± 100 (15)	1 ± 8 (3)	BDL	1052 ± 4929 (2440)	21 ± 77 (41)
Yellowish brown	9 ± 23 (17)	10 ± 17 (13)	2 ± 8 (9)	BDL	4016 ± 5915 (3752)	29 ± 68 (44)

We selected one parti-colored sample to further investigate the chemical differences between blue and yellow sapphires from this deposit. Mapping the chemistry of this sample showed that the only difference between the blue and yellow zones is the concentration of Ti, which is much higher in the

blue zones. This agrees, of course, with the color zoning: When there is more Ti than Mg, there will be excess Ti that can pair with Fe to create a blue color. In the yellow zone, the Ti content is less than Mg, and there is no Fe^{2+}-Ti^{4+} absorption, allowing the Fe^{3+} to produce a pure yellow color (see Table 3).

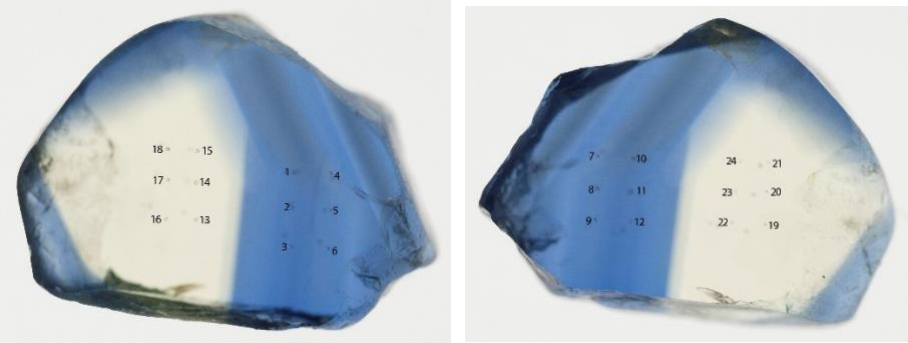

Figure 32. Sample showing the location of the 12 spots in each of the blue and yellow zones. Photographs by S. Engniwat.

Table 3. LA-ICP-MS results (in ppma) of the blue and yellow color zones in Australian sapphires.

	^{24}Mg	^{47}Ti	^{51}V	^{53}Cr	^{57}Fe	^{69}Ga
sp1	5	21	4	BDL	1596	30
sp2	5	23	4	BDL	1530	28
sp3	5	17	3	BDL	1457	29
sp4	4	13	4	BDL	1493	28
sp5	4	13	4	BDL	1431	28
sp6	4	16	4	BDL	1453	27
sp7	2	17	3	BDL	1293	25
sp8	3	16	3	BDL	1300	24
sp9	4	14	3	BDL	1336	24
sp10	2	17	3	BDL	1285	25
sp11	4	15	3	BDL	1314	24
sp12	4	15	3	BDL	1318	25
average	4 ± 1	17 ±4	3 ±0.3		1401 ± 370	27 ± 9
sp13	8	6	4	BDL	1676	31
sp14	8	6	4	BDL	1778	33
sp15	8	5	4	BDL	1723	32
sp16	8	6	4	BDL	1669	32
sp17	7	5	4	BDL	1683	31
sp18	8	6	4	BDL	1910	36
sp19	7	5	3	BDL	1534	28
sp20	7	5	3	BDL	1530	29
sp21	7	5	3	BDL	1548	27
sp22	7	6	4	BDL	1541	28
sp23	7	5	3	BDL	1471	27
sp24	7	4	4	BDL	1519	27
average	7 ± 0.4	5 ± 0.5	4 ± 0.3	BDL	1632 ± 130	30 ± 3

CONCLUSIONS

Despite their long history, Australian sapphires have remained underappreciated for a long time.

As with most basalt-related deposits, these sapphires are relatively high in Fe, resulting in the typical blue-green-yellow colors. The exact coloration is dependent on the availability of Ti to form pairs with Fe in the sapphire. A high amount of available Ti results in blue colors, while the absence of available Ti yields yellow colors.

Their inclusion scenes are dominated by various types of particles, with rutile particles being dominant in the blue stones. The rutile can occur as slender needles, fine milky clouds, or crosshatched particles which can aggregate in various formations. In green stones, the particles tend to be more iron-rich (ilmenite) and have a more irregular appearance. Solid crystals (mainly feldspar and opaque black crystals) and twinning features are commonly observed in all colors of sapphire. These inclusions are typical for all basalt-related sapphires, making them unreliable for geographic origin determination.

At first glance, trace element analysis appears to show significant overlap between different sources, but advanced statistical processing allows the confident separation of most basalt-related sources based on their chemical signature.

The renewed energy in the Australian sapphire industry, due to the emergence of some new players such as Fura Gems, will likely cause an increased enthusiasm for these gems.

ACKNOWLEDGMENTS

The authors thank Fura Gems for donating a selection of sapphires, both rough and cut, for this research project. Many thanks are also owed to the Australian sapphire mining community, which welcomed GIA during numerous field expeditions over the past decade.

We would also like to thank Charuwan Khowpong, Suwasan Wongchacree, Vararut Weeramongkhonlert, Ungkhana Atikarnsakul, and Titapa Tanawansombat for data collection.

ABOUT THE AUTHORS

Dr. Aaron Palke is senior manager of research at GIA's Carlsbad laboratory. Ms. Sudarat Saeseaw is senior manager of identification and Mr. Wim Vertriest is manager of field gemology, both based in Bangkok, Thailand. Queries about this work can be directed to apalke@gia.edu.

REFERENCES

Coldham T. (1985) Sapphires from Australia. *G&G*, Vol. 21, No. 3, pp. 130–146, http://dx.doi.org/10.5741/GEMS.21.3.130

Dunstan B. (1902) The sapphire fields of Anakie. Report, Geological Survey of Queensland, No. 172.

Emmett J.L., Stone-Sundberg J., Guan Y., Sun Z. (2017) The role of silicon in the color of gem corundum. *G&G*, Vol. 53, No. 1, pp. 42–47, http://dx.doi.org/10.5741/GEMS.53.1.42

Fukatsu N., Kurita N., Oka Y., Yamamoto S. (2003) Incorporation of hydrogen into magnesium-doped α-alumina. *Solid State Ionics*, Vol. 162-163, pp. 147–159, http://dx.doi.org/10.1016/S0167-2738(03)00218-2

Hughes R.W., Manorotkul W., Hughes E.B. (2017) *Ruby & Sapphire: A Gemologist's Guide*. RWH Publishing.

Moon A.R., Phillips M.R. (1991) Defect clustering in H, Ti:α-Al_2O_3. *Journal of Physics and Chemistry of Solids*, Vol. 52, No. 9, pp. 1087–1099, http://dx.doi.org/10.1016/0022-3697(91)90042-X

Sangsawong S., Pardieu V., Raynaud V., Engniwat S. (2016) "Punsiri"-type FTIR spectral features in natural yellow sapphires. *G&G*, Vol. 52, No. 3, pp. 325–327.

Sutherland F.L., Webb G.B. (2007) Australian sapphires and rubies. *Rocks & Minerals*, Vol. 82, No. 2, pp. 116–125, http://dx.doi.org/10.3200/RMIN.82.2.116-139

Sutherland F.L., Coenraads R.R., Abduriyim A., Meffre S., Hoskin P.W.O., Giuliani G., Beattie R., Wuhrer R., Sutherland G.B. (2015) Corundum (sapphire) and zircon relationships, Lava Plains gem fields, NE Australia: Integrated mineralogy, geochemistry, age determination, genesis, and geographical typing. *Mineralogical Magazine*, Vol. 79, No. 3, pp. 545 and 581, http://dx.doi.org/10.1180/minmag.2015.079.3.04